

A Highly Configurable Hardware/Software Stack for DNN Inference Acceleration

Suvadeep Banerjee, Steve Burns, Pasquale Cocchini, Abhijit Davare,
Shweta Jain, Desmond Kirkpatrick, Anton Sorokin, Jin Yang, Zhenkun Yang

Intel Labs

Abstract—This work focuses on an efficient design methodology for domain-specific accelerators. We employ an Agile development approach, with feature-by-feature enhancement of a vertical development stack. This development methodology has been applied to the TVM/VTA inference accelerator. Along the way, we have enhanced the VTA design space and enabled end-to-end support for additional workloads. This has been accomplished by augmenting the VTA micro-architecture and instruction set architecture (ISA), as well as by enhancing the TVM compilation stack to support a wide range of VTA configurations.

The VTA *tsim* implementation (CHISEL-based) has been enhanced with fully pipelined versions of the ALU and GEMM execution units. In *tsim*, memory width is now parameterized to range between 8-64 bytes per cycle. Field widths and ISA encoding have been made more flexible across multiple targets to support larger addressable scratchpads. A handful of new instructions have been added to enable new or faster functionality. These include: element-wise 8-bit multiplication to support depthwise convolution, load with a choice of pad values to support max pooling, and a clip instruction to support faster execution of a common pattern in ResNets. Support for additional layers, enhanced double buffering allowing for greater scratchpad utilization, and runtime enhancements to lower uop count have also been added.

A significant increase in performance is seen for the *tsim* target just using the fully pipelined versions of ALU and GEMM: $\sim 4.9x$ fewer cycles with minimal area increase to run ResNet-18 under the default configuration. By varying existing and newly added parameters, configurations featuring a further $\sim 11.5x$ decrease in cycle count at a cost of $\sim 12x$ greater area can be instantiated. Tens of intermediate points on the area-performance pareto curve are shown, showcasing the balance of execution unit sizing, memory interface width, and scratchpad sizing which is required to extract good performance from this relatively simple micro-architecture. Finally, VTA is now able to run Mobilenet 1.0 and all layers for ResNets, including the previously disabled pooling and fully connected layers.

The TVM/VTA architecture has always featured end-to-end workload evaluation on RTL in a matter of minutes. With our modifications, it now offers a much greater number of feasible configurations with a wide range of cost vs. performance. All capabilities mentioned here, and more, are available in open-source forks of the ‘tvm’ and ‘tvm-vta’ repositories. A subset of these capabilities have already been upstreamed.

Index Terms—TVM, VTA, inference, accelerator, compiler, agile design

I. INTRODUCTION

A. Motivation

Our motivation for exploring specialization of hardware (accelerators) to increase compute performance comes from some

of the early “dark silicon” work [1] [2], where the authors point out that while power has limited frequency scaling of general purpose compute, we have the opportunity to spend transistors on specialized processing for specific applications. Yet, the cost of developing new accelerators is too high. Moore’s law, which states that the cost per transistor decreases by 2x every process generation, does not help here unless the target accelerator has a very large market. For smaller markets, non-recurring engineering (NRE) costs dominate and any reduction of these costs could proportionally reduce per unit costs. Concentrating on new design methodologies that reduce NRE is therefore an important research direction. Hennessey and Patterson, in their 2018 Turing award paper [3], discuss this in their call for the development of Domain-Specific Accelerators.

Both software and hardware systems incur substantial NRE costs, as well as design and verification aspects of both. Developing design methodologies that jointly optimize both software and hardware is a focus of this work. In looking around for a domain to make our methodology research more concrete, we decided to explore inference accelerators for Machine Learning (ML), partly because of our initial exposure to DARPA’s RTML (Realtime ML) BAA [4] and early work with a performer on the project. In studying existing solutions to the problem, the TVM software stack and the VTA hardware accelerator looked promising as a good starting point for the methodology research we wanted to explore.

In looking at the existing solution, we found a fairly well developed software stack (TVM [5]) and an immature hardware implementation (VTA [6]). The hardware description was written in Chisel [7] which our team had existing experience with. However, it was incomplete in a variety of ways and did not compute the correct answers on at least one of the targeted FPGA platforms. So we decided to build up a development methodology to improve TVM/VTA so that it was as good as the underlying architecture would allow it to be. We wanted to show this with different amounts of hardware resources as well. This, in the end, involved correcting several things: 1) lack of parametrization, 2) poor end-to-end performance, 3) inflexible memory systems, 4) poor instruction sequences generated by the compiler (e.g., double buffering) and 5) non-optimal scratchpad sizes. To do all of this, we need to develop design methodologies along the way, including: 1) a test driven development (TDD) solution of developing hardware blocks, 2) visualization techniques for understanding the performance

of the system, 3) verification flows to determine where hardware implementation state diverges from software simulator state, 4) techniques to improve the compiler, 5) a continuous integration (CI) system to ensure software simulation, RTL simulation and FPGA simulation remained correct on each check-in, and 5) flows and methods for performing physical design as an ASIC.

B. Related Work

An early Domain Specific Language (DSL), Halide [8], introduced the important concept of separating specification of computation from the scheduling, which is dependent on the hardware target, an important advance in targeting workloads flexibly to different types of hardware acceleration. Recently, Deep Neural Networks have received great attention in DNN compilation stacks such as Tensorflow [9], PyTorch [10], MXNet [11] which map the deep learning operators to vendor-provided kernel libraries for execution on CPU and GPU hardware with high performance. Compiler frameworks such as Relay [12] and MLIR [13] have evolved for lowering the deep learning computations into these kernel libraries. Due to the high manual engineering effort required to develop and tune these libraries, there has been a recent proliferation of deep learning compilers that can automatically optimize the low-level implementation of tensor operators for a given accelerator design. One class are polymorphic compilers that pose program optimization as an integer linear programming problem, such as Tiramisu [14], FlexTensor [15], and Tensor Comprehensions [16]). Another class are those based on graph optimization techniques [17], [18] and auto-tuners such as Relay [12], OpenTuner [19], NeuroVectorizer [20] and AutoPhase [21] that achieve a certain level of auto-tuning. A final class, using a variety of schedule optimization techniques are Halide with its auto-schedulers [22]–[24], TVM [5] with AutoTVM and Anso [25].

DNNWeaver2 [26] is an early work in exploring software/hardware co-design in the DNN inference domain, serving as an inspiration for this work. On the hardware side we see innovations in flexible hardware construction languages that help generate new accelerators, like Chisel, PyMtl3 [27], Magma [28]. [29] has extended the targets of TVM to include a special inference hardware engine called Versatile Tensor Accelerator (VTA). Our effort is an extension of this TVM/VTA compiler/hardware stack.

II. TVM/VTA STACK OVERVIEW

A. Versatile Tensor Accelerator Microarchitecture

Figure 1 illustrates the Versatile Tensor Accelerator (VTA) hardware, a parameterized load-compute-store micro-architecture comprising fetch, load, compute, and store modules which use command queues to propagate inference compute tasks through the machine, and using scratch buffers to hold input, weight, and output (accumulate) data. The fetch module loads inference task micro-operation instructions from main memory and dispatches command sequences to the load, compute and store modules. The load module performs

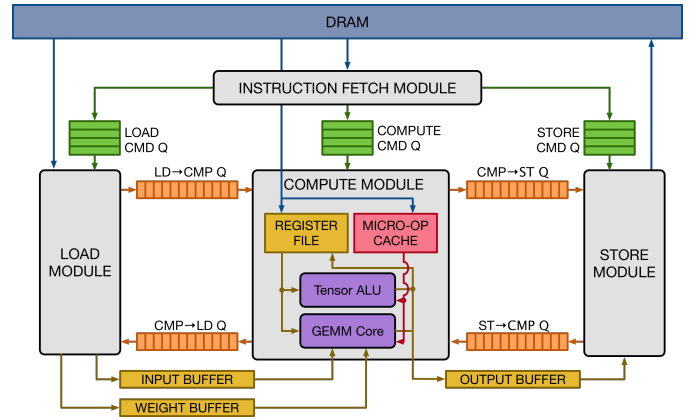


Fig. 1. VTA Microarchitecture [30]

strided memory access to load input, weight, and bias tensor tiles from DRAM into their on-chip buffers. The compute module contains a GEMM core for processing convolutional layers and an ALU for activation, normalization, and pooling layers. The GEMM unit as published has pipeline depth of 4 (single operand) or 5 (2 operands), the machine only can issue another GEMM instruction after completion resulting in an initiation interval (II) of 4. The ALU as published is not pipelined. Finally, the store module transfers the contents of the accumulate buffer to main memory upon completion of the inference task.

The load, compute, and store modules all obtain instructions from separate queues, and can execute in parallel. However, instructions within these queues may have read/write dependencies with instructions from other queues. Such dependencies are added by the compiler and enforced through the usage of the 4 dependency queues shown in Figure 1: *LD->CMP*, *CMP->LD*, *CMP->ST*, and *ST->CMP*. The compiler sets a subset of 4 dependency bits in each instruction: *pop prev*, *pop next*, *push prev*, and *push next*. Here, *prev* and *next* refer to the queues on the left and right sides, respectively, of the module which executes the instruction. *pop* commands block until a token is present in that queue before executing the instruction, while *push* commands insert a token into that queue. In essence, these 4 bits force sequential execution only when needed to avoid race conditions on the 3 shared resources which are touched by the modules: the input, weight, and output buffers. Setting extraneous dependency bits can result in longer cycle counts or even deadlock.

The VTA micro-architecture is modeled in a bit-accurate manner in two ways: *fsim*, which is a behavioral description of the machine and Chisel, which is a parameterized RTL description. The fundamental parameters of the machine are the BLOCK_IN and BATCH size of the input and BLOCK_OUT of the weight and accumulate tensors, as well as the size of the input, weight, and accumulate buffers. As published, the VTA hardware presumes a 64-bit databus for memory access, and the working Chisel configuration was limited to BLOCK_IN=BLOCK_OUT=16 with BATCH=1. The avail-

able ALU operations limit VTA operation to most, but not all, layers of ResNet inference workloads. Yet the RTL model is small enough to execute these workloads in minutes of simulation time, making it an interesting target for design space exploration.

B. Instruction Set

Instructions and micro-operations (uops) are used to program the VTA accelerator, and both were extended in order to allow greater microarchitectural flexibility. New instructions and variants were also added to enable additional functionality.

The VTA ISA contains 5 instructions: GEMM, ALU, LOAD, STORE, and FINISH. The GEMM and ALU instructions are *compute* instructions and each is associated with a sequence of uops. Each uop in the sequence holds base addresses for the scratchpads that are read/written within the loops which characterize the instruction. The LOAD and STORE instructions are capable of being executed in parallel with *compute* instructions, and are not associated with uops. By default, each instruction is 128 bits wide while each uop is 32 bits wide.

Instructions and uops are emitted by the runtime, while they are consumed by each of the hardware targets (*fsim*, *tsim*, etc). Both sides need to have a common understanding of the structure and semantics, while hardware needs to instantiate the structures (e.g. queues) and decoders which are required to process the instructions and uops. Due to the two-level breakdown of VTA into a runtime along with hardware, the upper compiler/runtime interface can remain more insulated from ISA changes.

Our goals to change the shapes of tensors processed by GEMM and ALU instructions and modify the sizes of scratchpads naturally result in field width changes within both instructions and uops.

For uops, we also extended the size of uops since not enough spare bits were available. Wider uops can support wider fields, allowing larger scratchpads, but also require additional storage and memory bandwidth.

For instructions, we retained the 128-bit width as a constant. Permitting increased width for certain fields uses up spare bits. After exhausting available spare bits, we resorted to shrinking other field widths in order to fit within the instruction width constraint.

A JSON configuration file is the only compile-time construct consumed by the compiler, runtime, as well as all hardware targets. Variable field widths can be captured in the JSON file. New JSON parameters need to be handled across multiple languages. Compile-time checks - such as ensuring instruction width constraints are not violated - need to be implemented as well.

C. Compiler

The software stack for targeting the VTA hardware starts with ingesting deep learning models expressed in frameworks such as Pytorch [10], TensorFlow [9] and MxNet [11] into Relay [12] IR (Intermediate Representation) for representing

computational graphs. The TVM compiler decomposes the workload into appropriate VTA-compatible operator schedules where the operators are further partitioned by loop manipulations into VTA hardware intrinsics such as GEMM/ALU or DMA load/store. The VTA compilation stack includes a software defined runtime that performs JIT compilation of the TVM compiler generated API calls for creating the final instruction sequence.

For extracting high performance out of VTA, the TVM compiler utilizes the decoupled access-execute philosophy [31] by exploiting thread parallelism. The virtual thread injection pass of the TVM compilation stack partitions schedule tasks into different execution contexts such that load, store and compute operations can concurrently execute. This double buffering is effective in hiding the memory latency such that one half of the scratchpad is used by DMA load/store, where the compute module operates on the other half. The compiler manages this fine-grained parallelism by analyzing subsequent load, compute and store nodes in the IR to determine the local buffer addresses being used. This information is used to create the memory access and compute instruction JIT calls with requisite *push* and *pop* tokens injected into these calls.

The SW stack implements a SW-defined runtime system that manages heterogeneous execution of workloads on CPU and VTA. Instead of the TVM compiler directly generating code for the VTA target, the runtime exposes a high-level API of hardware intrinsic calls that the compiler can lower schedules onto. The JIT runtime creates the instruction stream from the compiler generated recipe by managing DRAM load/store and managing micro-kernel generation. The runtime interprets the *push* and *pop* dependency tokens inserted by the compiler between instruction calls to control the sequential execution of the instructions. The flexibility of the JIT runtime allows layers of a deep network to be either executed on the CPU or offloaded to the VTA, thus ensuring that a DNN can be executed on VTA even if the accelerator doesn't support all layers.

III. DEVELOPMENT METHODOLOGY

In this section, we provide an overview of our Agile development methodology: how we decide to implement a new incremental feature and how we ensure it is implemented correctly.

A. Performance Analysis and Visualization

Given an existing, mostly working TVM/VTA repository, we now had the problem of analyzing the existing performance and determining what simple changes could be made to improve the design. We created two simple visualizations to help with this analysis: 1) a roofline chart [32] which can show in a single diagram how closely a computation fully utilizes the available compute resources and memory bandwidth; and 2) an activity visualization of the three loosely-coupled processes in VTA (*load*, *compute*, and *store*). Figure 2 shows our Roofline chart for a variety of scratchpad sizes, number of compute units, and memory bandwidths. Figure 3 shows that all three

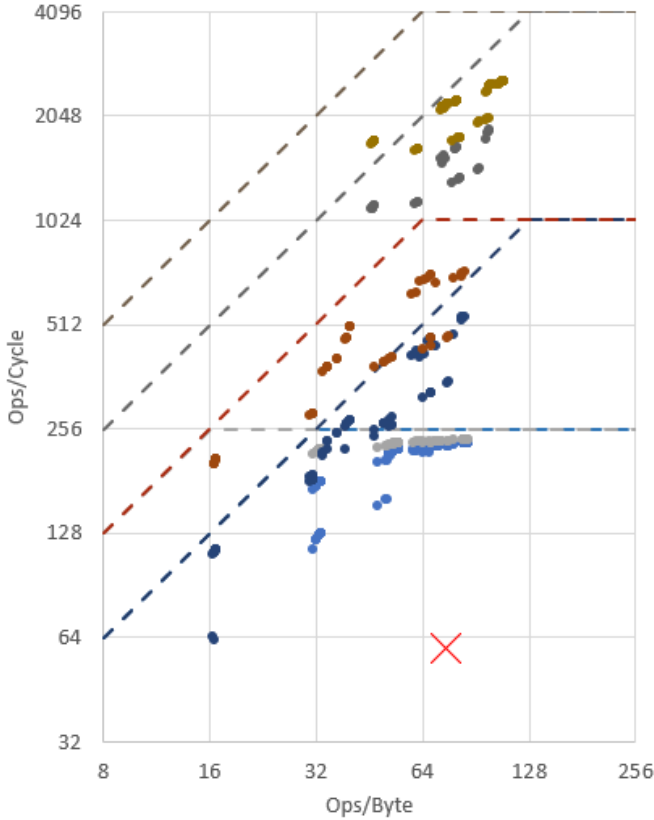


Fig. 2. Roofline Chart: This is a log-log chart with Ops/Byte on the x-axis and Ops/Cycle on the y-axis. The horizontal dashed lines represent compute bounds based on the number of simultaneously operable compute units. The diagonal dashed lines correspond to memory bandwidth limit (the intercept with the vertical line Ops/Byte = 8 corresponds to the bandwidth in Bits/Cycle).

processes can run concurrently in a balanced design. Figure 4 show a more detailed view from which one can easily see dependencies between the VTA processes.

B. Always-alive Modeling

The TVM/VTA inference stack spans many layers: workloads, compiler, runtime, behavioral model, and RTL. These layers are implemented in a variety of languages. Development may be carried out by non-overlapping groups of people. Feature enhancements to one layer may not be visible with end-to-end workload evaluation unless other layers are modified in tandem. Conversely, unanticipated degradation in workload performance may occur due to relatively minor changes in a given layer. Reducing the time required to see the effects of a given change motivated the development of an always-alive model.

In a traditional ‘waterfall’ development methodology, many features can be in flight simultaneously. The initial decomposition of functionality into features is carried out at an early stage while the integration of features takes place as one of the last stages during the development process. During feature development, implementations are usually tested in

isolation, for instance with unit tests written against the feature specification, in order to facilitate parallel development. Since integration and end-to-end testing are deferred, information gleaned from these activities cannot drive significant implementation changes without schedule slip.

In this work, we follow the Agile approach, where integration occurs frequently, giving fast insights into the impact of a particular feature. This low-latency feedback requires automation of integration and end-to-end evaluation. If manual effort were required, its aggregate cost across the development process would be too high. At the beginning of development, it is important to bootstrap a baseline vertical stack which exercises as much end-to-end behavior as possible. It is expected that these capabilities will be enhanced and expanded during the development process: integration and evaluation should be incrementally developed features.

For the TVM/VTA inference stack, end-to-end evaluation involves both functional and performance aspects. Running inference on input image(s) and comparing the labels against expected results for both the behavioral and RTL targets gives us an indication of functional correctness. Performance counters in the RTL model tracked over time help us understand the performance impact of various features.

C. Dynamic Trace-based Validation

Central to any agile development methodology is the ability to quickly identify and correct any functional, performance defects present in the design at the end of frequent integration runs. Indeed, without such a capability, verification and validation tasks would quickly become a challenging bottleneck increasing design turn-around-time to unacceptable levels.

To ensure a sufficiently high degree of functional coverage, a regression suite composed of several representative end-to-end tests was setup to run during continuous integration cycles, with test content highly parameterized and varying from a few instructions to entire inference workloads.

All tests were run for 4 supported targets of the VTA accelerator [29], all sharing the same common runtime introduced earlier:

- *fsim*: C++ behavioral model. Low design complexity as compared to other targets.
- *bsim*: HeteroCL [33] behavioral model.
- *tsim*: Cycle accurate model simulating Chisel-generated RTL using Verilator [34].
- *de10nano*: FPGA emulation model using the DE10-Nano board [35] (based on the Intel Cyclone V FPGA), running a cycle accurate model synthesized from Chisel-generated RTL.
- *pyngq*: FPGA emulation target using the Pynq board [36] (based on the Xilinx Zynq FPGA), running a VTA cycle accurate module synthesized from a C++ High Level Synthesis model using Vivado HLS [37].

When a test failed to produce the expected result for any given target, the test was rerun in *trace mode* under the same conditions and for all supported targets, producing a configurable dump of architectural states. The trace produced



Fig. 3. Process Utilization Visualization for a complete ResNet-18 workload. The three bars correspond to the *load*, *compute* and *store* processes. This computation is compute bound because both *load* and *store* are idle for significant amounts of time. The red sections of *compute* correspond to GEMM activity and the green sections to ALU activity.

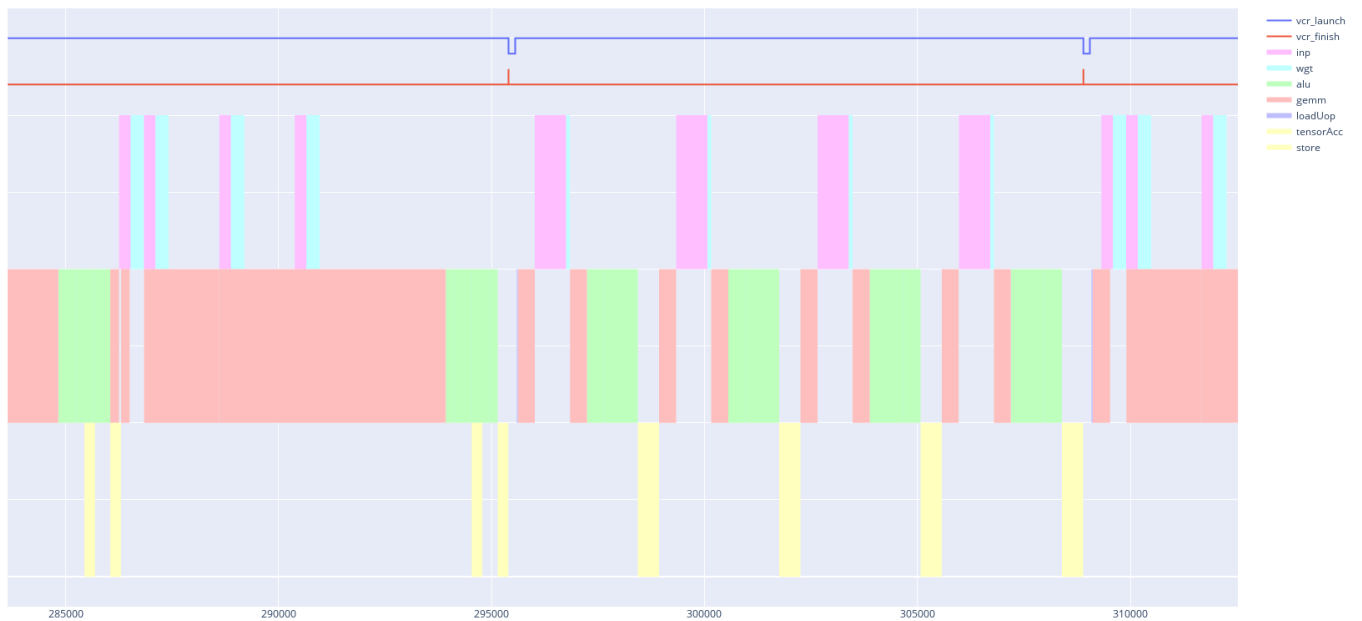


Fig. 4. Process Utilization Visualization for three partial layers of the ResNet-18 workload. The complete layer (between the red ticks, *vcr_finish*) shows a sequential ordering between the *load*, *compute* and *store* activities. This layer could likely be improved by double buffering, allowing, for example, *load* and *compute* activities to run concurrently. The previous layer (to the left of the first red tick), shows this overlap and is likely implemented using double buffering.

by the failing target was then compared to the trace produced by another passing target. A detailed comparison pinpointed the location in the trace where the behavior of the failing target diverged from that of the passing target. The divergence point was then used to cross-reference the failing target code and find the location of the defect.

The methodology required the instrumentation of arbitrary architectural states across behavioral and RTL targets written in different languages, i.e. C++, Python, Scala. To this purpose, a trace manager module was developed in each language featuring a common interface that allowed for the unambiguous specification of the same architectural states to be monitored and traced.

For flexibility and ease of use, tracing was parameterized through the use of user selectable *trace modes* allowing the generation of traces with different levels of granularity, both in time and across runtime and architectural state spaces. For instance, generating traces for a specific scratchpad SRAM memory, at specific time events in the GEMM or ALU units.

This methodology was found to be very effective at quickly locating defects especially when comparing the *tsim* cycle accurate RTL target versus the *fsim* behavioral reference C++ target, through a careful selection of relevant runtime and architectural states with invariant properties exhibited in both models.

D. Unit Testing

Unit testing provides the finest granularity and fastest testing capabilities for test-driven RTL design. It is based on Chisel Testers. Chisel Testers provide a library for functional testing at the lowest design hierarchy level that gives fast turnaround time for a cycle-accurate simulation. It also provides cycle-accurate traces for power and performance analysis. Chisel Iotesters PeekPokeTester is used to communicate with RTL. Iotesters provide connection with three simulation backends. Treadle is a FIRRTL level simulator. It provides performance comparable with verilator and has a very short spin-up time. Treadle cannot handle black box Chisel modules which are provided as Verilog sources; therefore, vcs or verilator should be used to run tests with memory compiler hard IP blocks. Chisel Verilog compiler can replace memories with external reference to macro memories if it is required for further physical synthesis flow. A Chisel-based macro memory compiler is used to select and connect memory compiler hard IP blocks and provide macro memory blocks for given memory configurations. PeekPokeTester is driven by Scala test driver code that can communicate at different levels of VTA hierarchy. The highest level of communication is VTAShell AXI interface level. Another level is Core vme/vcr communication level. To drive both levels, a Scala code to create instructions/opcodes/data is used. It is also used to encode execution parallelism ordering. A GEMM multiplication with double buffering in scratchpad and ALU load-operate-store with different padding can be executed at those levels for all feasible configurations automatically. A multiple read/write requests memory model with a constant latency

is implemented. Tests created for original configuration drive development and validation of a new functionality. While the largest configurations of VTA could take several minutes to compile Verilog from Chisel sources, it is more practical to run tests first on a smaller VTA which can be compiled in less than a minute. The simulation time of most unit tests is less than a minute that puts checking of a small feature in a category of almost interactive development.

IV. RESULTS

A. Performance Analysis Driven Improvements

We realized the main hardware related performances improvements in a greedy incremental way. Performance analysis, in particular utilization charts like Figure 3, showed that the design was compute bound on the ResNet-18 workload.

1) *Pipelining the GEMM Unit*: Analysis showed that a significant amount of time was being spent in the GEMM unit. While the matrix-vector units were fully pipelined, they were only being used once every fourth cycle. The main state machine for the *compute* unit was sequencing through four states: *fetch uop*, *fetch data*, *MAC*, and *writeback* for each computation. Since the control flow is completely determined, a very simple pipelining strategy transforms this to initiation interval (II) equal to 1. The basic idea is to have a single control unit generating a sequence of three dimensional loop indices. We then pipeline the UOP lookup, the weight and input scratchpad lookups, and finally the vector-matrix product calculation. A simple inflight queue is used to flush the pipeline after completion of each instruction (which typically takes hundreds of cycles to complete).

RTL changes were done locally to the *TensorGEMM* block using handcrafted unit tests following a TDD methodology. While these tests passed, full end-to-end integration tests (on some subset of the layers of Resnet-18) failed. The case of this failure was an address staging bug in another unit (*LoadUop*) which was uncovered now because uops are being fetched every cycle instead of once every four cycles. (This bug would have been easy to catch using the dynamic tracing facility, which was not available when this RTL work was performed). Careful study of signal traces was required to root cause and correct this error. Significant work went into developing a complete Chisel-based testbench of the *TensorGEMM* including not only tests on the sequence of indices generated, but also on the values produced by the matrix-vector units. This testbench included a Scala-based model of the *LoadUop* block [considered to be part of the environment to *TensorGEMM*] and was not helpful in finding the bug.

2) *Pipelining the ALU Unit*: With the GEMM unit no longer the bottleneck, we decided to similarly improve performance of the ALU which had an II of either 4 or 5 (depending on whether one or two operands were needed). Initial analysis suggested that little gain could be achieved by improving this unit that was rarely used. This analysis mistakenly assumed an II=1. Redoing it we discovered using the utilization diagrams shown in Figure 3 that approximately 50% improvement was possible at least for some of the ResNet-18 layers.

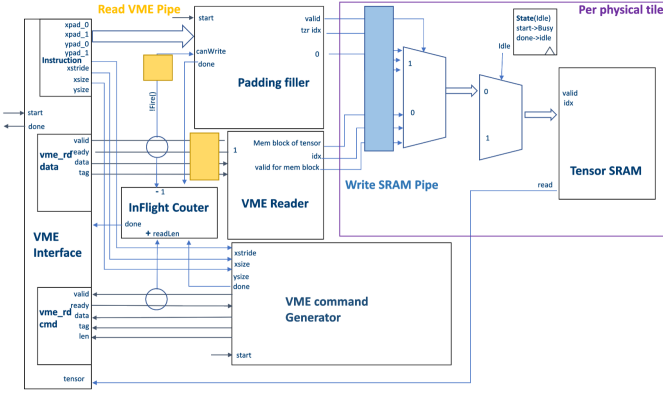


Fig. 5. Separate Load CMD and VME Data transfer to process parallel load requests. Padding fill is executed when VME Reader is not busy.

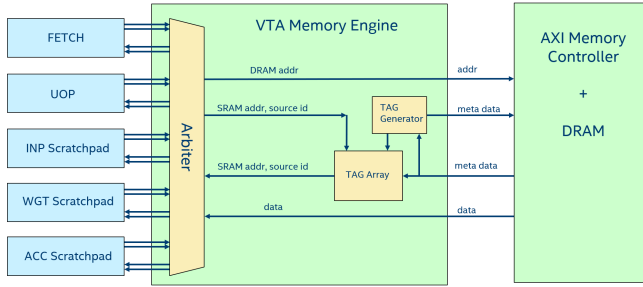


Fig. 6. VTA Memory Engine enhanced with multiple outstanding requests and out-of-order completion. This micro-architecture allows multiple memory load requests to be inflight simultaneously. Complex metadata (scratchpad identifiers and addresses) are stored locally in the VME and only a tag is sent as metadata to the AXI memory controller. When the tag returns, it is used to recover the metadata and then send the load response data to the correct source scratchpad. The maximum number of inflight requests is limited by the size of this tag buffer and the capacity of the AXI memory controller.

Again, RTL changes were done locally to the *TensorALU* block. This time, handcrafted unit tests following the TDD methodology were only developed for the index generation logic. The final pipeline was $\Pi=2$ for two operand instructions (because the accumulator register file only allows one read access per cycle) and $\Pi=1$ for one operand (immediate) instructions. Final testing was done at the integration-test level using the dynamic tracing capability to find some wiring errors at the datapath level. This hybrid approach (Chisel-based tests for control streams and dynamic tracing for data steering) is recommended as a good balance that utilizes the best of both testing methodologies.

3) *Expanding the memory interface*: Existing VTA memory interface functionality is limited by 64-bit data interface. This limitation bounds computation by memory transfer. By expanding memory data interface to handle 64, 128, 256, 512-bit AXI data width, we achieved balanced compute-data transfer VTA performance for GEMM with up to 4K MAC operations. TensorLoad functionality was generalized for all communications with VME. Two transfer modes were defined with respective implementations. Narrow data interface mode is used when AXI data width is less than destination data

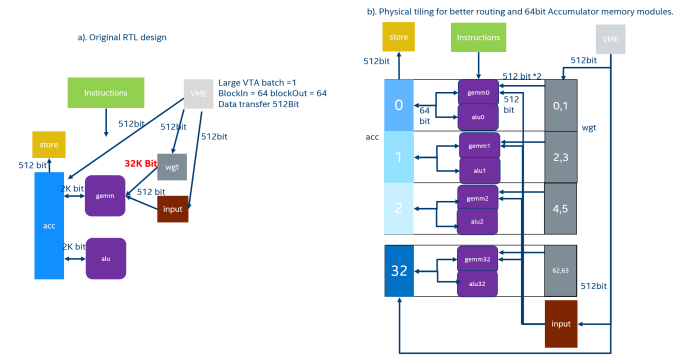


Fig. 7. a). Original RTL design. All similar functionality is grouped leading to 32K bit data read interface. b). Tile is grouped around minimum GEMM functionality. TensorLoad is spread over whole die area.

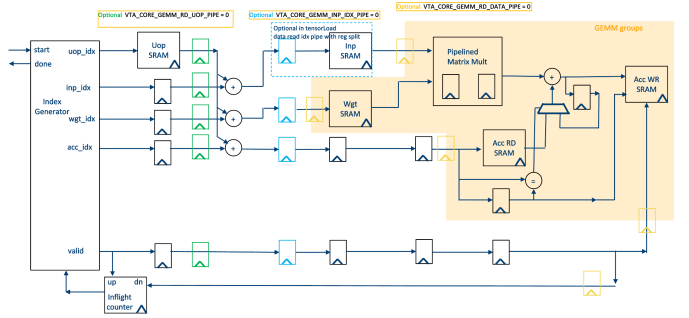


Fig. 8. Distance from instruction decoder and to Input and Store scratchpads may require pipe stages for better timing.

type width. Wide interface is for AXI data width wider than destination type width. For example, 128-bit AXI data loader into 32-bit UOP buffer uses wide loader implementation and can write 4 UOPs per cycle. 128-bit AXI data to 256 byte WGT scratchpad tensor loader uses a narrow type implementation with 16 AXI pulses per tensor load. The ratio of sizes between AXI and destination data should be power of 2. Instruction load is configured as 64/128/256/512 AXI data bits to 64-bit tensor loader with 128-bit tensor read interface. This allows to require 64-bit instruction address alignment instead of 128. Communication was separated into independent command generation and a data transfer interface communication as shown in Figure 5. The number of inflight AXI data load requests is controlled by VME module. VTA core TensorLoad module issues AXI data load requests which are queued by VME. Each AXI request is accompanied by a scratchpad destination address which is stored by VME together with request id. VME uses AXI id to identify request data destination and initiates data burst transfer, sends data and provides stored destination scratchpad address. A wide TensorLoad implementation also uses a destination address and a mask to mark valid bytes. The new functionality is summarized in Figure 6.

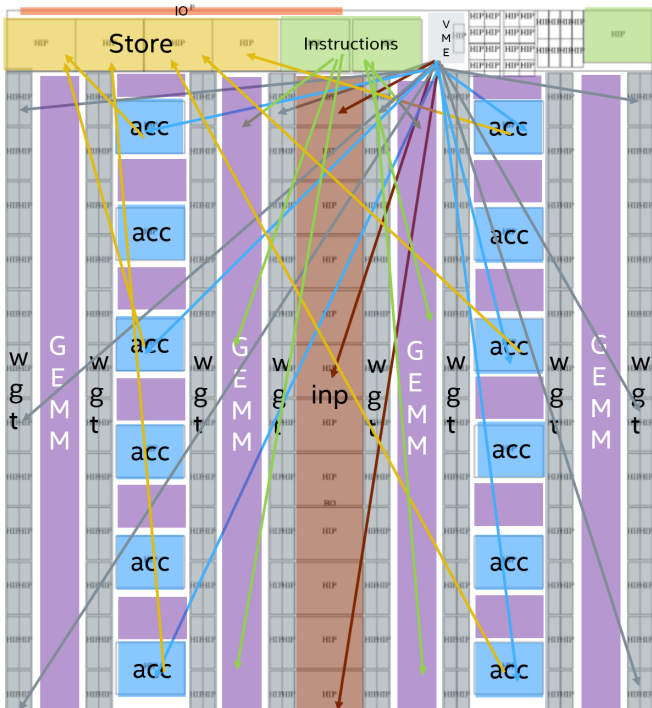


Fig. 9. Weight, Input, Accumulator scratchpad memory modules are not grouped together. Large TensorLoad data transfer distance requires pipe stages.

B. Flexible Floorplans

A floorplanning Python library was created to support generation of multiple floorplans for different VTA configurations. Floorplan generator allows definition of layout objects with design sub-hierarchy name, width, height, and orientation. At bottom leaf level of floorplan hierarchy, we have macro modules which are usually instances of memory modules. They have width and height provided by tech description. Design sub-hierarchy can have placement bounds. Each floorplan has a definition in a form of a Python class hierarchy and implementation generated by running that program. Floorplanner provides capability to instantiate arrays of floorplan instances and flip individual objects if required. Result visualization and overlap/spacing, unique instance name checks are also provided. The original VTA design hierarchy is built around GEMM/ALU/INP/WGT/ACC/OUT objects communicating with each other. Physical size of those object should be considered if VTA configuration is large enough for communication lines to require buffering. Another problem is a routing congestion. Wide WGT and ACC data buses produce too much congestion if floorplan placement bounds are based on original design hierarchy. Physical design tools use design instances to define physical constraints. Multiple runs of physical flow are required to converge on timing and routing congestion metrics. Floorplanner allows to write a flexible program to generate multiple hierarchies of different size and orientation of objects with reuse of existing sub-hierarchies. A better design hierarchy built around ACC scratchpad value was found

as shown in Figure 7. A center of this structure is an ACC memory module which is used to store GEMM/ALU result. GEMM/ALU read and write this module, so their logic is placed nearby, and it is timing critical and not being spread too far. Tested VTA configurations have BATCH of 1 or 2 which BLOCK_IN and BLOCK_OUT can be quite large up to 64. It means that WGT scratchpad memory bit width can be quite large and only a portion of it is used to get each ACC value. In a case of BATCH 1, BLOCK_IN 64 and BLOCK_OUT of 64 it means 512 bit of WGT scratchpad are used to compute one and only one value of ACC. All 512 bits from INP scratchpad are used to get 64 different values of ACC. It makes sense to place a portion of WGT scratchpad close to respective ACC module. Not much could be done to distribute INP scratchpad. OUT scratchpad writing can be pipelined and that scratchpad can be placed anywhere depending on available space. The same UOP and instruction memory data is used in each GEMM/ALU and can be placed anywhere and buffered/pipelined. Major modules of design cannot be placed as separate instances as GEMM/ALU/ACC/WGT/INP content overlap each other all over die area.

C. Wire Pipelining

1) *GEMM pipelining*: GEMM and ALU have functionality which is common for every value to be calculated and a unique functionality which is specific for each result value as shown in Figure 8. The result of common part calculation is delivered to each memory module and it is buffered and pipelined as read UOP and generate index pipes. WGT reading part of GEMM/ALU compute and ACC writing was grouped around ACC value and optimized for minimum delay and pipe stages. GEMM/ALU units were grouped into groups with as many units as needed to complete computation in one cycle while they all are fed by UOPs/Instruction/INP data from some distant source.

2) *Scratchpad load pipelining*: Scratchpad loading is a delivery of VME data or scratchpad tensor size number of bits to a respective memory module as shown in Figure 9. In many VTA configurations WGT/ACC scratchpads are distributed all over die area and INP scratchpad is quite large. Data from VME cannot be delivered to them in one cycle and requires construction of a buffering tree. The original design hierarchy was changed and WGT/ACC/INP were split into groups. WGT/ACC groups are based on ACC value calculation code and how much can be computed at one logic stage.

D. Compiler Modifications

We modified the compiler for lowering all deep learning layers to different configurations of VTA with high performance. We introduce a heuristic-guided analytical scheme called *Tiling Parameter Search (TPS)* for mapping deep learning operators such as standard convolution and depthwise convolution to different VTA configurations. We modify the TVM IR pass related to threading for improving double buffering of the GEMM and LOAD operations in VTA. In addition, we enable the execution of depthwise convolution

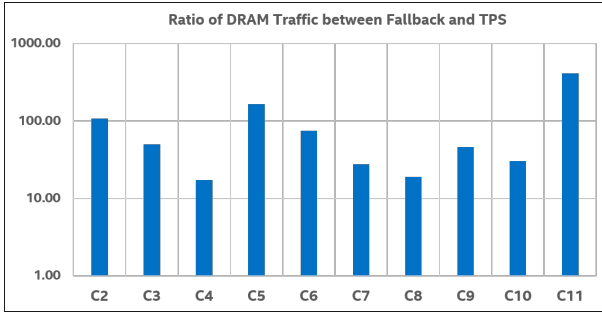


Fig. 10. With TPS, DRAM byte transfer is reduced by 20x-400x for different convolution layers on BLOCK=32 configuration

and dense layers in VTA, thus providing full support for ResNet and MobileNet workloads in VTA.

1) *Tiling Parameter Search*: The TVM compiler creates *schedules* for representing tensor operators as a blueprint for lowering the computation to VTA through tensorize intrinsics and memory load/store instructions. The convolution schedule is expressed in a fixed scheduling template with a sequence of program transformation primitives such as loop reordering, tiling and threading. Different choices of the tiling parameters modify the data access patterns of the schedule and alters the ordering of memory accesses and compute unit execution, thereby directly affecting the performance. AutoTVM [38] and Ansor [25] provide an automated search process to optimize program schedules. Both these schemes use a cost model that requires collecting performance metrics of candidate schedules from a hardware platform. During the VTA design enhancement, we required fast discovery of high-performance convolution implementations on different VTA configurations, for which we used TPS.

For a given convolution schedule and a VTA configuration, we express the bytes transferred from DRAM to scratchpads as an analytical cost function of the tiling parameters, as expressed in Appendix A. We use this cost function and scratchpad size constraints to rapidly explore the tiling parameter space and optimize a convolution schedule for a given VTA configuration. Without the TPS algorithm, the default behavior of the TVM-VTA stack is to use a fallback schedule for convolution that guarantees compilability of a deep learning workload on any VTA configuration by ensuring minimal use of local scratchpad at the expense of high DRAM byte transfer. Using the TPS algorithm, we are able to reduce the DRAM byte transfer by 2-3 orders of magnitude as shown in Figure 10. We plot the ratio of DRAM traffic (in bytes) created by the fallback schedule and the TPS-generated schedule for ResNet-18 convolution layers C2-C11 on a VTA configuration with BLOCK_IN=BLOCK_OUT=32.

2) *Double Buffering*: The double buffering implementation of VTA divides each of the input, weight and accumulator scratchpads into two different logical chunks for separate load and compute access. While one half of the scratchpads is loaded with data from DRAM, the compute units (GEMM and ALU) operate on data present in the other half. The existing

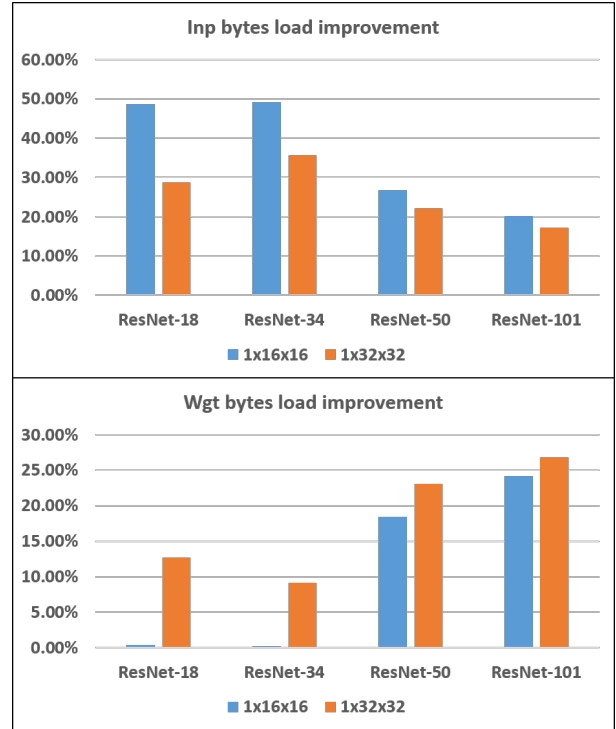


Fig. 11. Reduction in bytes loaded from DRAM to scratchpad (1x16x16 config implies VTA batch=1, block-in=16, block-out=16)

implementation of the TVM compiler’s virtual threading pass fetches redundant data from DRAM to the two halves of the scratchpad, thus failing to exploit data reuse. For example, with two halves of input and weight scratchpads represented as I_1, I_2 and W_1, W_2 , two chunks of input and weight data represented as d_{i1}, d_{i2} and d_{w1}, d_{w2} , the compiler loads d_{i1} and d_{w1} into I_1 and W_1 respectively. After the load completes, the GEMM module works on I_1 and W_1 , whereas the load module loads d_{i1} and d_{w2} into I_2 and W_2 . This causes redundant load of d_{i1} twice. We modified the thread injection IR pass to automatically identify the redundant loads in alternative memory load threads and reuse the d_{i1} for the second GEMM by modifying the uop access pattern sequence from $(I_1, W_1), (I_2, W_2), (I_1, W_1), (I_2, W_2)$ to $(I_1, W_1), (I_1, W_2), (I_2, W_1), (I_2, W_2)$. This modification reduces power consumption by suppressing redundant memory loads and for memory-bound workloads, this improves throughput as well.

Figure 11 shows the reduction in byte transfer from DRAM to input and weight scratchpads for 4 different ResNets on 2 VTA configurations. For a given workload on a particular VTA configuration, the total reduction of bytes loaded from DRAM is $\approx 50\%$, as the modification removes every other load of a data chunk. This, in turn, reduces the total power consumption by removing the redundant memory loads.

Figure 12 shows the reduction in cycle count for 4 ResNets on 3 different VTA configurations. For small networks (ResNet 18 and 34), the cycle count increases on small VTA configurations (256 MAC units) because of the higher uop memory

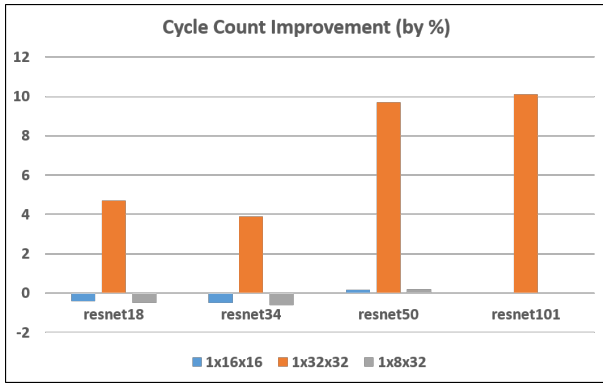


Fig. 12. Reduction in cycle count due to double buffering improvement

loads. As these configurations are not memory-bound (and compute-bound instead), suppressing redundant DRAM loads doesn't improve throughput. For larger networks (ResNet 50 and 101) on compute-heavy configurations, reducing memory loads improves the performance by reducing the cycle count by $\approx 10\%$.

3) *Depthwise Layers*: Depthwise separable convolution layers proposed in MobileNet [39] architecture reduce the computational intensity of the convolution operation by factoring the convolution into depthwise and pointwise convolutions. The depthwise convolution applies a single filter to each individual channel, thus removing the channel-wide summation of standard convolution. This requires modifications in the TVM-VTA stack to support depthwise convolution layers. VTA's GEMM unit is a fused multiply-accumulate (MAC) unit that sums the partial product of input and weight over the input channels. As depthwise convolution doesn't sum the input-weight product over the input channels, we chose to utilize the VTA's ALU instead of the GEMM unit to execute depthwise convolution workloads. We created a new ALU opcode [40], [41] for element-wise multiplication and mapped a new schedule that divides up the depthwise computation into multiplications and additions. With this change, we are able to execute depthwise layers and in consequence, MobileNet network in VTA.

E. End-to-end networks

We created VTA schedules for average and max pooling layers by utilizing the ALU unit. With these modifications, we are able to execute the full ResNets from the 2nd convolution layer (1st convolution layer being channel-light at 3 channels is executed on the CPU by default [6]) to the final fully-connected layer at the end. Similarly, we are able to execute the end-to-end MobileNet1.0 network with the added feature of executing depthwise layers on VTA. The capability of running end-to-end networks on the accelerator helps in targeted evaluation of accelerator design choices as we minimize the execution of DNN layers on CPU.

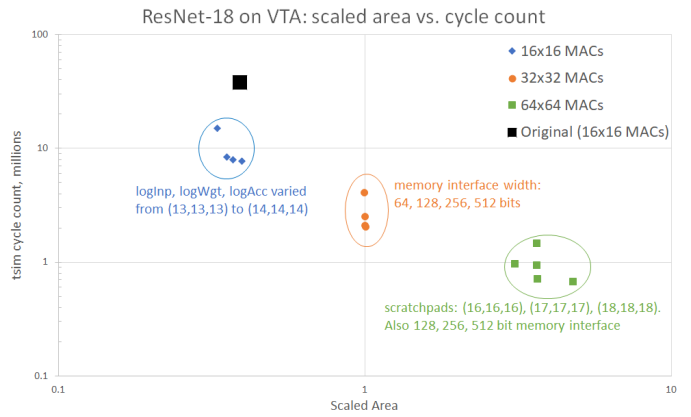


Fig. 13. Cycle count vs. Scaled Area for a complete ResNet-18 Workload. The three ovals encapsulate points from 3 different MAC shapes: 4x4, 5x5, and 6x6. Within each oval, memory interface width and/or scratchpad sizes are varied.

F. Large design space

One of the goals of our work was to expand the size of the design space. A larger hardware design space obviously offers alternative points on the performance-cost pareto curve. However, another benefit is that it may help lower NRE costs if certain points have unanticipated synthesis or APR challenges. Such benefits can only be realized if implemented throughout the stack.

The expanded design space we have enabled for TVM/VTA is summarized in Figure 13. The original TVM/VTA stack we started with had a cycle count of 38 million cycles for this ResNet-18 workload, with scaled area roughly equal to the other points with 4x4 MACs.

Overall, we can see that scaled area varies by an order of magnitude among these points, while the cycle counts vary by a slightly greater range. Scratchpad size is the main contributor to scaled area, while the cycle count metric is affected by a variety of factors. Overall, a balancing of the compute (captured by GEMM shape), memory bandwidth (captured by memory interface width), and scratchpad size (captured by the addressable bits for all scratchpads) is necessary to decrease the cycle count for this design. Note that the relative impact of these factors also depends on the workload being executed.

G. Continuous Integration

A key part of ensuring an always-alive model is to build a continuous integration (CI) system which is capable of exercising cross-layer workloads on each commit. Figure 14 details the workloads, targets and approximate runtimes of the CI system we built for the TVM/VTA stack. The 3 lower ovals show the 3 main targets which are exercised (*fsim*, *tsim*, and *DE10 FPGA*) by cross-layer workloads. The small upper oval covers unit testing, which is populated by CHISEL unit tests which are initially used for test-driven design.

The parameter setting, TVM framework build, runtime build, and equality checking stages are shared amongst all targets. The common stage which consumes the largest run-

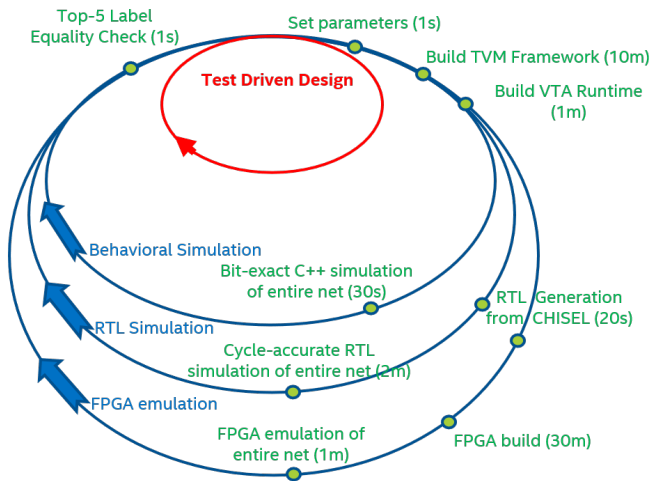


Fig. 14. Continuous Integration quickly and automatically exercises cross-layer workloads.

time is building the TVM framework, which takes around 10 minutes. However, TVM framework build is independent of VTA, and we rarely made any modifications to it, meaning this stage could be skipped during most CI runs.

We did not anticipate the high simulation speed we were able to reach with *tsim*. Using the verilog path, RTL simulation of VTA for several million cycles only took a few minutes. End-to-end runs with accurate cycle counts were added to the CI pipeline for several representative neural network workloads. This also allowed us to gauge the performance impact of feature additions. Moreover, when backend runs were carried out later, we were able to retroactively judge area vs. performance tradeoffs.

The role of the behavioral simulator *fsim* changed as well. The main value of the *fsim* model was no longer its fast simulation speed, but instead its relative simplicity. Functional discrepancies introduced by the CHISEL micro-architecture implementation in *tsim* were much easier to debug with the help of the *fsim* behavioral reference model. Dynamic trace-based validation capabilities were often used to find the earliest divergence between the *fsim* and *tsim* models, lowering debug time.

The usage of the *DE10 FPGA* target changed from our initial plan as well. Our early investment into this platform was driven by the expectation that long traces were only realistically possible on an FPGA platform, and that running such long traces would be a frequent activity. However, the fast *tsim* runtime confirmed the latter yet rejected the former assumption. The relatively long FPGA build time was unable to be amortized among the end-to-end runs since RTL simulation was fast enough for the relatively small number of neural networks we targeted. In addition, multi-core RTL simulation was easily able to scale unlike the device-limited FPGA scaling.

In our CI usage, the FPGA platform became more of an integration target: were the assumptions regarding the environment

made by the CHISEL model accurate? We were able to find memory access timing bugs in the CHISEL implementation which were only exercised in the context of a realistic FPGA platform and not in the context of the simpler environmental model used by RTL simulation. In this debug, the dynamic trace instrumentation capabilities were able to assist us to debug to a narrow window in time where the traces started to diverge.

H. Open source contributions

The results described in this section have been open sourced in forked repositories [40] [41]. Portions of this work related to ALU and GEMM pipelining and memory bus width parameterization have been merged into upstream *tvm* and *tvm-vta* repositories. These changes only involve the CHISEL-generated-RTL (*tsim*) target. Modifications to the instruction set architecture to support larger field widths have not yet been upstreamed since they affect additional targets. In addition, compiler modifications needed to support additional layers and networks are not yet upstreamed.

V. CONCLUSIONS AND FUTURE WORK

Motivated by reducing the NRE cost for hardware accelerators, we decided to take a hardware/software co-design approach to enhancing the TVM/VTA inference accelerator. Our methodology for enhancement was based on incremental changes to features up and down the stack combined with always-alive modeling. We were able to achieve significant increases in performance and vastly expand the size of the design space. Moreover, the end-to-end workload evaluation time is low enough (a few minutes) that our enhanced stack can assist in adjacent development activities, an example is exploration of the DNN architecture itself.

The design space exposed by our configurable inference accelerator can be jointly explored with the inference workload to be run on the accelerator. Strategies to automatically discover better neural network architectures [42] have emerged in the past few years. While initially focused on abstract computation costs, optimization of inference latency for a given hardware target has been explored in [43]. When such exploration is done at design time on a configurable hardware target, a large set of additional options become available.

As we have seen, legal parameter values for our configurable inference accelerator have complex constraints. Such constraints may be related to synthesis or place-and-route effects, available process-specific macros, instruction set limitations, and compiler features. Resolving these issues to create a denser design space may be possible with additional time, design effort, or increased hardware fabrication cost. The most expedient design space, however, is likely sparse. This design space sparsity is ill-suited to current hardware-workload co-optimization approaches. Based on this motivation, we have developed a pragmatic yet effective approach based on realizable hardware in [44] to optimize both latency and energy-delay-product metrics.

REFERENCES

- [1] H. Esmailzadeh, E. Blem, R. S. Amant, K. Sankaralingam, and D. Burger, "Dark silicon and the end of multicore scaling," in *2011 38th Annual International Symposium on Computer Architecture (ISCA)*, 2011, pp. 365–376.
- [2] M. B. Taylor, "Is dark silicon useful? harnessing the four horsemen of the coming dark silicon apocalypse," in *DAC Design Automation Conference 2012*, 2012, pp. 1131–1136.
- [3] J. L. Hennessy and D. A. Patterson, "A new golden age for computer architecture," *Communications of the ACM*, vol. 62, no. 2, pp. 48–60, 2019.
- [4] "DARPA RTML BAA," <https://www.grants.gov/web/grants/view-opportunity.html?oppId=313859>, accessed: 2021-09-03.
- [5] T. Chen, T. Moreau, Z. Jiang, L. Zheng, E. Q. Yan, H. Shen, M. Cowan, L. Wang, Y. Hu, L. Ceze, C. Guestrin, and A. Krishnamurthy, "TVM: An automated end-to-end optimizing compiler for deep learning," in *OSDI*, 2018.
- [6] T. Moreau, T. Chen, Z. Jiang, L. Ceze, C. Guestrin, and A. Krishnamurthy, "VTA: an open hardware-software stack for deep learning," *arXiv preprint arXiv:1807.04188*, 2018.
- [7] J. Bachrach, H. Vo, B. Richards, Y. Lee, A. Waterman, R. Avizienis, J. Wawrzyniek, and K. Asanović, "Chisel: Constructing hardware in a scala embedded language," in *DAC Design Automation Conference 2012*, 2012, pp. 1212–1221.
- [8] J. Ragan-Kelley, C. Barnes, A. Adams, S. Paris, F. Durand, and S. Amarasinghe, "Halide: A language and compiler for optimizing parallelism, locality, and recomputation in image processing pipelines," in *Proceedings of the 34th ACM SIGPLAN Conference on Programming Language Design and Implementation*, ser. PLDI '13. New York, NY, USA: Association for Computing Machinery, 2013, p. 519–530. [Online]. Available: <https://doi.org/10.1145/2491956.2462176>
- [9] M. Abadi, P. Barham, J. Chen, Z. Chen, A. Davis, J. Dean, M. Devin, S. Ghemawat, G. Irving, M. Isard, M. Kudlur, J. Levenberg, R. Monga, S. Moore, D. G. Murray, B. Steiner, P. Tucker, V. Vasudevan, P. Warden, M. Wicke, Y. Yu, and X. Zheng, "Tensorflow: A system for large-scale machine learning," in *Proceedings of the 12th USENIX Conference on Operating Systems Design and Implementation*, ser. OSDI'16. USA: USENIX Association, 2016, p. 265–283.
- [10] A. Paszke, S. Gross, F. Massa, A. Lerer, J. Bradbury, G. Chanan, T. Killeen, Z. Lin, N. Gimelshein, L. Antiga, A. Desmaison, A. Kopf, E. Yang, Z. DeVito, M. Raison, A. Tejani, S. Chilamkurthy, B. Steiner, L. Fang, J. Bai, and S. Chintala, "Pytorch: An imperative style, high-performance deep learning library," in *Advances in Neural Information Processing Systems 32*. Curran Associates, Inc., 2019, pp. 8024–8035. [Online]. Available: <http://papers.nips.cc/paper/9015-pytorch-an-imperative-style-high-performance-deep-learning-library.pdf>
- [11] T. Chen, M. Li, Y. Li, M. Lin, N. Wang, M. Wang, T. Xiao, B. Xu, C. Zhang, and Z. Zhang, "MXNet: A flexible and efficient machine learning library for heterogeneous distributed systems," 2015.
- [12] J. Roesch, S. Lyubomirsky, L. Weber, J. Pollock, M. Kirisame, T. Chen, and Z. Tatlock, "Relay: a new ir for machine learning frameworks," *Proceedings of the 2nd ACM SIGPLAN International Workshop on Machine Learning and Programming Languages*, Jun 2018. [Online]. Available: <http://dx.doi.org/10.1145/3211346.3211348>
- [13] C. Lattner, M. Amini, U. Bondhugula, A. Cohen, A. Davis, J. Pienaar, R. Riddle, T. Shpeisman, N. Vasilache, and O. Zinenko, "Mliir: A compiler infrastructure for the end of moore's law," 2020.
- [14] R. Baghdadi, J. Ray, M. B. Romdhane, E. D. Sozzo, A. Akkas, Y. Zhang, P. Suriana, S. Kamil, and S. Amarasinghe, "Tiramisu: A polyhedral compiler for expressing fast and portable code," in *2019 IEEE/ACM International Symposium on Code Generation and Optimization (CGO)*, 2019, pp. 193–205.
- [15] S. Zheng, Y. Liang, S. Wang, R. Chen, and K. Sheng, "Flextensor: An automatic schedule exploration and optimization framework for tensor computation on heterogeneous system," in *Proceedings of the Twenty-Fifth International Conference on Architectural Support for Programming Languages and Operating Systems*, ser. ASPLOS '20. New York, NY, USA: Association for Computing Machinery, 2020, p. 859–873. [Online]. Available: <https://doi.org/10.1145/3373376.3378508>
- [16] N. Vasilache, O. Zinenko, T. Theodoridis, P. Goyal, Z. DeVito, W. S. Moses, S. Verdoolaege, A. Adams, and A. Cohen, "Tensor comprehensions: Framework-agnostic high-performance machine learning abstractions," *CoRR*, vol. abs/1802.04730, 2018. [Online]. Available: <http://arxiv.org/abs/1802.04730>
- [17] Y. Liu, Y. Wang, R. Yu, M. Li, V. Sharma, and Y. Wang, "Optimizing CNN model inference on cpus," in *2019 USENIX Annual Technical Conference (USENIX ATC 19)*. Renton, WA: USENIX Association, Jul. 2019, pp. 1025–1040. [Online]. Available: <https://www.usenix.org/conference/atc19/presentation/liu-yizhi>
- [18] Z. Zheng, P. Zhao, G. Long, F. Zhu, K. Zhu, W. Zhao, L. Diao, J. Yang, and W. Lin, "Fusionstitching: Boosting memory intensive computations for deep learning workloads," *CoRR*, vol. abs/2009.10924, 2020. [Online]. Available: <https://arxiv.org/abs/2009.10924>
- [19] J. Ansel, S. Kamil, K. Veeramachaneni, J. Ragan-Kelley, J. Bosboom, U.-M. O'Reilly, and S. Amarasinghe, "Opentuner: An extensible framework for program autotuning," in *2014 23rd International Conference on Parallel Architecture and Compilation Techniques (PACT)*, 2014, pp. 303–315.
- [20] A. Haj-Ali, N. K. Ahmed, T. Willke, Y. S. Shao, K. Asanovic, and I. Stoica, "Neurovectorizer: End-to-end vectorization with deep reinforcement learning," ser. CGO 2020. New York, NY, USA: Association for Computing Machinery, 2020, p. 242–255. [Online]. Available: <https://doi.org/10.1145/3368826.3377928>
- [21] A. Haj-Ali, Q. J. Huang, J. Xiang, W. Moses, K. Asanovic, J. Wawrzyniek, and I. Stoica, "Autophase: Juggling hls phase orderings in random forests with deep reinforcement learning," in *Proceedings of Machine Learning and Systems*, I. Dhillon, D. Papailiopoulos, and V. Sze, Eds., vol. 2, 2020, pp. 70–81. [Online]. Available: <https://proceedings.mlsys.org/paper/2020/file/4e732ced3463d06de0ca9a15b6153677-Paper.pdf>
- [22] A. Adams, K. Ma, L. Anderson, R. Baghdadi, T.-M. Li, M. Gharbi, B. Steiner, S. Johnson, K. Fatahalian, F. Durand, and J. Ragan-Kelley, "Learning to optimize halide with tree search and random programs," *ACM Trans. Graph.*, vol. 38, no. 4, Jul. 2019. [Online]. Available: <https://doi.org/10.1145/3306346.3322967>
- [23] T.-M. Li, M. Gharbi, A. Adams, F. Durand, and J. Ragan-Kelley, "Differentiable programming for image processing and deep learning in Halide," *ACM Trans. Graph. (Proc. SIGGRAPH)*, vol. 37, no. 4, pp. 139:1–139:13, 2018.
- [24] R. T. Mullapudi, A. Adams, D. Sharlet, J. Ragan-Kelley, and K. Fatahalian, "Automatically scheduling halide image processing pipelines," *ACM Trans. Graph.*, vol. 35, no. 4, Jul. 2016. [Online]. Available: <https://doi.org/10.1145/2897824.2925952>
- [25] L. Zheng, C. Jia, M. Sun, Z. Wu, C. H. Yu, A. Haj-Ali, Y. Wang, J. Yang, D. Zhuo, K. Sen, J. E. Gonzalez, and I. Stoica, "Ansor: Generating high-performance tensor programs for deep learning," in *14th USENIX Symposium on Operating Systems Design and Implementation (OSDI 20)*. USENIX Association, Nov. 2020, pp. 863–879. [Online]. Available: <https://www.usenix.org/conference/osdi20/presentation/zheng>
- [26] H. Sharma, J. Park, D. Mahajan, E. Amaro, J. K. Kim, C. Shao, A. Mishra, and H. Esmailzadeh, "From high-level deep neural models to fpgas," in *Microarchitecture (MICRO), 2016 49th Annual IEEE/ACM International Symposium on*. IEEE, 2016, pp. 1–12.
- [27] S. Jiang, P. Pan, Y. Ou, and C. Batten, "Pymlt3: A python framework for open-source hardware modeling, generation, simulation, and verification," *IEEE Micro*, vol. 40, no. 4, pp. 58–66, 2020.
- [28] R. Bahr, C. Barrett, N. Bhagdikar, A. Carsello, R. Daly, C. Donovick, D. Durst, K. Fatahalian, K. Feng, P. Hanrahan, T. Hofstee, M. Horowitz, D. Huff, F. Kjolstad, T. Kong, Q. Liu, M. Mann, J. Melchert, A. Nayak, A. Niemetz, G. Nyengele, P. Raina, S. Richardson, R. Setaluri, J. Setter, K. Sreedhar, M. Strange, J. Thomas, C. Torg, L. Truong, N. Tsiskaridze, and K. Zhang, "Creating an agile hardware design flow," in *Proceedings of the 57th ACM/EDAC/IEEE Design Automation Conference*, ser. DAC '20. IEEE Press, 2020.
- [29] T. Moreau, T. Chen, Z. Jiang, L. Ceze, C. Guestrin, and A. Krishnamurthy, "VTA: an open hardware-software stack for deep learning," *CoRR*, vol. abs/1807.04188, 2018. [Online]. Available: <http://arxiv.org/abs/1807.04188>
- [30] T. Moreau, T. Chen, L. Vega, J. Roesch, E. Yan, L. Zheng, J. Fromm, Z. Jiang, L. Ceze, C. Guestrin et al., "A hardware-software blueprint for flexible deep learning specialization," *IEEE Micro*, vol. 39, no. 5, pp. 8–16, 2019.
- [31] J. E. Smith, "Decoupled access/execute computer architectures," *SIGARCH Comput. Archit. News*, vol. 10, no. 3, p. 112–119, Apr. 1982. [Online]. Available: <https://doi.org/10.1145/1067649.801719>

- [32] S. Williams, A. Waterman, and D. Patterson, "Roofline: an insightful visual performance model for multicore architectures," *Communications of the ACM*, vol. 52, no. 4, pp. 65–76, 2009.
- [33] Y.-H. Lai, Y. Chi, Y. Hu, J. Wang, C. H. Yu, Y. Zhou, J. Cong, and Z. Zhang, "HeteroCl: A multi-paradigm programming infrastructure for software-defined reconfigurable computing," in *Proceedings of the 2019 ACM/SIGDA International Symposium on Field-Programmable Gate Arrays*, ser. FPGA '19. New York, NY, USA: Association for Computing Machinery, 2019, p. 242–251. [Online]. Available: <https://doi.org/10.1145/3289602.3293910>
- [34] W. Snyder. (2021) Welcome to verilator. [Online]. Available: <http://https://www.veripool.org/verilator/>
- [35] Intel. (2021) Terasic de10-nano kit. [Online]. Available: <https://www.intel.com/content/www/us/en/developer/topic-technology/edge-5g/hardware/fpga-de10-nano.html>
- [36] Xilinx. (2021) Pynq: Python productivity. [Online]. Available: <http://pynq.io>
- [37] Synopsys. (2021) Vivado 2021.1 - high-level synthesis (c based). [Online]. Available: <https://www.xilinx.com/support/documentation/navigation/design-hubs/dh0012-vivado-high-level-synthesis-hub.html>
- [38] T. Chen, L. Zheng, E. Yan, Z. Jiang, T. Moreau, L. Ceze, C. Guestrin, and A. Krishnamurthy, "Learning to optimize tensor programs," 2019.
- [39] A. G. Howard, M. Zhu, B. Chen, D. Kalenichenko, W. Wang, T. Weyand, M. Andreetto, and H. Adam, "Mobilenets: Efficient convolutional neural networks for mobile vision applications," *CoRR*, vol. abs/1704.04861, 2017. [Online]. Available: <http://arxiv.org/abs/1704.04861>
- [40] "TVM open source contributions," https://github.com/pasqoc/incubator-tvm/tree/il_contrib_0421.
- [41] "TVM-VTA open source contributions," https://github.com/pasqoc/incubator-tvm-vta/tree/il_contrib_0421.
- [42] B. Zoph and Q. V. Le, "Neural architecture search with reinforcement learning," 2017.
- [43] H. Cai, L. Zhu, and S. Han, "Proxylessnas: Direct neural architecture search on target task and hardware," *arXiv preprint arXiv:1812.00332*, 2018.
- [44] Y. Akhauri, A. Niranjan, J. P. Muñoz, S. Banerjee, A. Davare, P. Cochini, A. A. Sorokin, R. Iyer, and N. Jain, "Rhnas: Realizable hardware and neural architecture search," <https://arxiv.org/abs/2106.09180>, 2021.

APPENDIX

A. Tiling Parameter Search

A convolution layer is characterized by batch b , activation height h and width w , kernel height kh and kw , activation channels fi , output channels fo , padding height ph and width pw , stride height sh and width sw . The VTA GEMM unit is characterized by batch b_{VTA} , block-in factor BI and block-out factor BO . The output height oh and width ow are calculated as

$$oh = \left\lfloor \frac{h + 2 \times ph - kh}{sh} \right\rfloor + 1, ow = \left\lfloor \frac{w + 2 \times pw - kw}{sw} \right\rfloor + 1 \quad (1)$$

For tensorizing the convolution to VTA GEMM intrinsics, the input and output channels are chunked up by block-in and block-out respectively, to create 2 additional dimensions in the tensor operations as $di = \frac{fi}{BI}$ and $do = \frac{fo}{BO}$. The scheduling template applies tilings to 5 different dimensions to create outer and inner tiling pairs. A dimension of size n can be tiled as (n_o, n_i) , where $n_o \times n_i = n$. The 5 tiling dimensions are

$$\begin{aligned} \frac{b}{b_{VTA}} &\rightarrow (tb_o, tb_i), oh \rightarrow (th_o, th_i) \\ ow &\rightarrow (tw_o, tw_i), do \rightarrow (tco_o, tco_i) \\ di &\rightarrow (tci_o, tci_i) \end{aligned}$$

In addition, two virtual thread dimensions are defined along output channel and input height dimension as oc_n and h_n that control the double buffering of weight or input scratchpad respectively. The virtual threading parameters can be either 1 or 2 to indicate whether double buffering is enabled or not. Both the values can't be simultaneously 2. The TPS algorithm is a constrained cost minimization problem, where the cost is the DRAM byte transfer and the constraints are the scratchpad usage. It can be expressed as

$$\begin{aligned} \min(l_{inp} + l_{wgt} + l_{acc}) \\ u_{inp} &\geq 0 \\ u_{wgt} &\geq 0 \\ u_{acc} &\geq 0 \end{aligned} \quad (2)$$

where l_{inp} , l_{wgt} and l_{acc} are the bytes loaded into input, weight and accumulator scratchpads respectively. The under-utilization factors u_{inp} , u_{wgt} and u_{acc} ensure that a candidate tiling scheme is able to fit data fetches within the scratchpad sizes. Each of these factors are expressed through tiling parameters, workload parameters and VTA configuration parameters as,

$$\begin{aligned} l_{inp} &= tb_o \times \frac{th_o}{h_n} \times \frac{tco_o}{oc_n} \times tw_o \times tci_o \times s_{inp} \\ l_{wgt} &= tb_o \times \frac{th_o}{h_n} \times \frac{tco_o}{oc_n} \times tw_o \times tci_o \times s_{wgt} \\ l_{acc} &= tb_o \times th_o \times tw_o \times fo \end{aligned}$$

where s_{inp} and s_{wgt} are the usages of the input and weight scratchpads and expressed as

$$\begin{aligned} s_{inp} &= tb_i \times \frac{fi}{tci_o} \times \left(\left\lfloor \frac{\frac{h}{th_o} + 2 \times ph - kh}{sh} \right\rfloor \times sh + kh \right) \\ &\times \left(\left\lfloor \frac{\frac{w}{tw_o} + 2 \times pw - kw}{sw} \right\rfloor \times sw + kw \right) \\ &\times b_{VTA} \times BI \times oc_n \times h_n \\ s_{wgt} &= \frac{fo}{BO} \times \frac{fi}{BI} \times kh \times kw \times BO \times BI \\ &\times oc_n \times h_n \end{aligned} \quad (3)$$

The under-utilization factors of the scratchpads are calculated as the difference between the scratchpad size and the corresponding usage. With c_{inp} , c_{wgt} and c_{acc} as the capacity of the input, weight and accumulator scratchpads, the factors u_{inp} , u_{wgt} and u_{acc} are expressed as,

$$\begin{aligned} u_{inp} &= c_{inp} - s_{inp} \\ u_{wgt} &= c_{wgt} - s_{wgt} \\ u_{acc} &= c_{acc} - s_{acc} \end{aligned} \quad (5)$$

with the accumulator usage s_{acc} expressed as

$$\begin{aligned} s_{acc} &= \left(\frac{\frac{b}{b_{VTA}} \times \frac{fo}{BO} \times oh \times ow \times b_{VTA} \times BO}{tb_o \times tco_o \times th_o \times tw_o} + \frac{fo \times b}{tb_o \times tco_o} \right) \\ &\times oc_n \times h_n \end{aligned} \quad (6)$$

The TPS algorithm exhaustively enumerates all the configurations in the tiling parameter space and finds the optimized schedule by evaluating the constrained cost minimization problem expressed in (2).